The Golgi-associated microtubule cross-linking protein MTCL2 promotes the multipolar extension of dendrites in cerebellar granule neurons.

Running title: MTCL2 promotes multipolar extension of dendrites.

Mari Minekawa and Atsushi Suzuki*

Molecular Cellular Biology Laboratory, Yokohama City University Graduate School of Medical Life Science, 1-7-29 Suehiro-cho, Tsurumi-ku, Yokohama 230-0045, Japan.

* Corresponding author: Atsushi Suzuki; email: abell@yokohama-cu.ac.jp

Keywords: MTCL2, Golgi apparatus, cerebellar granule neurons, dendrite, polarity

Abstract

The dynamic regulation of neuronal polarity is essential for establishing neural networks during brain development. The primary culture of rodent neurons recapitulates several aspects of this polarity regulation and thus provides powerful tools for revealing the cellular and molecular mechanisms underlying axon specification and neuronal migration. However, little is known about how preexisting bipolarity breaks to form multipolar dendrites. Here, we demonstrated that the Golgi-associated, microtubule (MT) cross-linking protein MTCL2 plays an essential role in this type of polarity change observed in the differentiation of cerebellar granule neurons (CGNs). MTCL2 is highly expressed in CGNs and exhibited gradual accumulation in dendrites in parallel to their polarity development. MTCL2 depletion resulted in the generation of longer and fewer dendrites by suppressing the bipolar-to-multipolar transition of dendrite extension observed in the normal polarization process. During this process, the Golgi apparatus changes its localization from the base of the preexisting bipolar neurites to the lateral or apical side of the nucleus, where it associates closely with the MT cage wrapping the nucleus. The resulting upward extension of the Golgi apparatus is tightly coupled with randomization of its position in x-y plane. Knockdown/rescue experiments demonstrated that MTCL2 promotes these changes in Golgi position in an MT- and Golgi-binding activity-dependent manner. These results suggest that MTCL2 promotes the development of multipolar short dendrites by sequestering the Golgi apparatus from the base of preexisting neurites, enabling its random movements around nuclei.

Introduction

Neurons are highly polarized cells in the human body that develop two types of functionally distinct processes: thin long axons and short dendrites. To establish an elaborate neuronal circuit in the brain, most neurons gradually complete their neuronal polarity in parallel with migration to an appropriate region during development.

Several pioneering studies have demonstrated that neurons isolated from embryonic or neonatal rodent brains can recapitulate similar polarization processes *in vitro* (Dotti et al., 1988; Fletcher and Banker, 1989; Powell et al., 1997). During dissociation, neurons lose their original neurites and initially exhibit a round shape. However, they maintain their ability to develop axons and dendrites even in the absence of specific cell-to-cell contacts or extracellular matrix molecules. These results demonstrate that the essential polarization process is intrinsically programed in neurons, at least, in part. Rodent hippocampal neurons are the most intensively studied model systems for studying neuronal polarity (Tahirovic and Bradke, 2009). The cells isolated from the late embryo first develop a multipolar morphology with several short neurites decorated with dynamic growth cones at their tips, exhibiting rapid growth and retraction. The remarkable polarization event occurs 1-2 days after plating when one of these initial neurites begins to grow rapidly and become a thin, long axon. Thereafter, the remaining short neurites developed into dendrites (>3-4 days). Most studies in this field have focused on the initial event breaking the first multipolarity because similar axon specification processes have been observed in the developing neocortex and hippocampus *in vivo* (Kitazawa et al., 2014; Miyata et al., 2004; Noctor et al., 2004). Accumulating evidence has established that rearrangement of the actin cytoskeleton and microtubules and regulation of their dynamic properties are crucial targets of cell-polarizing signals elicited stochastically or by extrinsic cues (Tahirovic and Bradke, 2009; Takano et al., 2015; Witte et al., 2008) .

Dissociation cultures of cerebellar granule neurons (CGNs) represent an alternative system for studying neuronal development, which exhibit a unique polarization process that differs from that of hippocampal neurons (Powell et al., 1997; Solecki et al., 2006;

Tahirovic and Bradke, 2009; Zmuda and Rivas, 1998). CGNs are isolated from the postnatal cerebellum of rodents (Hatten and Heintz, 1995; Krämer and Minichiello, 2010), which is still under development (Millen et al., 1994). In the early postnatal cerebellum, CGNs are located in the external granular layer and develop bipolar axons parallel to the pial surface. They do not extend the multipolar dendrites that appear in later stages when they migrate to their destination, namely, the internal granular layers. Reflecting this *in vivo* situation, when early postnatal CGNs are isolated and seeded in culture dishes, they first exhibit unipolar and/or bipolar neurites. Thereafter, their final morphology, with a thin long axon and several short dendrites extending into multiple directions, gradually developed (Powell et al., 1997; Zmuda and Rivas, 1998). This process is completely different from that observed in neocortex or hippocampus neurons, which start from multipolar polarity when cultured in *vitro* (Tahirovic and Bradke, 2009). This characteristic development process of CGNs provides a unique and useful system *in vitro* for studying another aspect of neuronal polarization, namely how neurons break the preexisting bipolarity to develop dendrites in multiple directions. In fact, early studies on CGNs have focused on this issue and demonstrated the possibility that randomization of the positions of the Golgi apparatus and centrosomes is involved in this process (Zmuda and Rivas, 1998). However, due to the lack of subsequent studies that extended these initial insights, the cellular and molecular mechanisms underlying this bipolar-to-multipolar transition remain largely unknown, although the cultured CGNs themselves have been intensively utilized to clarify the molecular mechanisms for neuronal migration (Kawaji et al., 2004; Nagata and Nakatsuji, 1990; Rao et al., 2016; Rivas and Hatten, 1995; Solecki et al., 2004), axonogenesis (Arakawa et al., 2003; Oishi et al., 2021), and dendritogenesis (Huang et al., 2007; Litterman et al., 2011; Tan et al., 2013).

MTCL2 (previously, also called SOGA1) is a novel microtubule-associated protein that we have recently identified and characterized (Matsuoka et al., 2022). It is a long-extending protein with a molecular mass of 180 kDa that crosslinks MTs by interacting with them through its C-terminal region and by dimerizing through its central coiled-coil region. The N-terminal portion of the coiled-coil region exhibits another activity in association with the

Golgi membrane by interacting with CLASPs and Giantin. These activities enable MTCL2 to exert its unique function as a crosslinker of MTs on the Golgi membrane. We demonstrated that through this function, MTCL2 accumulates MTs around the Golgi apparatus, thereby promoting the compact assembly of Golgi stacks into a Golgi ribbon. A wound-healing assay using a cultured cell line suggested that the functions of MTCL2 are essential for maintaining directional migration (Matsuoka et al., 2022).

In this study, we demonstrated that MTCL2 is highly expressed in CGNs *in vivo*. In cultured CGNs, MTCL2 exhibited gradual accumulation in dendrites in parallel to polarity development. MTCL2 depletion resulted in abnormally polarized CGNs with longer and fewer dendrites, and several experiments including live-cell imaging revealed that MTCL2 is required for the bipolar-to-multipolar transition of dendrite extensions. Immunofluorescence analysis and knockdown/rescue experiments indicated the role of MTCL2 in sequestering the Golgi apparatus from the base of bipolar neurites to the MT cage wrapping the nucleus, which gradually develops during CGN differentiation. The importance of the MT cage in the change of the Golgi position and the bipolar-to-multipolar transition of dendrite extension was also demonstrated by inhibiting the LINC complex, which provides links between the nuclear membrane and MTs. Taken together, these results demonstrate a novel role for MTCL2 in promoting the bipolar-to-multipolar transition of dendrite extension through its ability to link the Golgi apparatus and MTs.

Results

MTCL2 is preferentially enriched in the dendrites of cerebellar granule neurons

Previously, our western blot analysis of mouse tissue extracts revealed preferential expression of MTCL2 in the lung, testis, ovary, cerebrum, and cerebellum (Matsuoka et al., 2022). Consistently, public data bases for mRNA expression in human and mouse organs (https://www.ebi.ac.uk/gxa/home and https://www.proteinatlas.org) as well as *in situ* hybridization data of the mouse brain (https://mouse.brain-map.org/) (Fig. S1A) suggest high expression of MTCL2 in the cerebellum. Our immunostaining analysis of the mouse brain further revealed its preferential expression in granule cells and, at a lesser degree, in Bergman glial cells (Fig. 1A ; A. Suzuki, unpublished observation). Interestingly, MTCL2 signals were not detected in Purkinje cells in our immunostaining data, as well as in the public *in situ* hybridization data of the mouse brain (Fig. S1A). This provided a sharp contrast to its paralogue, MTCL1, which is expressed and plays critical functions in Purkinje cells (Fig. S1B) (Satake et al., 2017). Based on these results, we analyzed MTCL2 functions in cerebellar granule neurons (CGNs) using dissociated cultures of mouse CGNs (see Materials and Methods) (Krämer and Minichiello, 2010; Powell et al., 1997).

When isolated CGNs cultured for 5 days *in vitro* (DIV5) were subjected to immunofluorescence analysis, anti-MTCL2 antibody revealed strong signals in cell bodies and some restricted neurites (Fig. 1B). These signals disappeared after MTCL2 knockdown (Fig. S2), indicating the genuine localization of endogenous MTCL2 in CGNs. The neurites exhibiting a strong MTCL2 signal corresponded well to MAP2-positive dendrites (Fig. 1B), and the intensities of MTCL2 and MAP2 staining were highly correlated (Fig. 1C: Pearson correlation coefficient was 0.83). Because MTCL2 also showed weak localization to MAP2-negative thin axons (Fig. 1B,C), we concluded that MTCL2 is preferentially enriched in but not restricted to MAP2-positive dendrites in differentiated CGNs.

We next examined when MTCL2 began to exhibit dendrite enrichment during CGN

polarization. For this purpose, we compared the intensities and patterns of the immunostaining signals of dephosphorylated tau (tau1), MAP2, and MTCL2 in CGNs cultured for 1–5 days (Mandell and Banker, 1996). Consistent with previous reports, CGNs extended tau1-positive short processes 1 day after seeding (Fig. 1D, arrowheads) (Zmuda and Rivas, 1998), most of which acutely elongated after DIV2 and gradually became axon-like neurites with longer and thinner morphologies. On the other hand, MAP2 signals were very weak until DIV2 but began to be detected in short neurites after DIV3. During these developmental processes, MTCL2 signals were detected even at DIV1 or 2, with comparable levels (~80%) observed at DIV5 (Fig. 1D,E). The high expression of MTCL2 during the early stage of polarization was confirmed by western blot analysis (Fig. 1F). At these initial stages, signals were detected in cell bodies and in some tau1-positive initial neurites (Fig. 1D, arrowheads). However, around DIV3-4 when MAP2-positive neurites appeared, MTCL2 gradually exhibited selective enrichment in these neurites (Fig. 1D,E). These results suggest that MTCL2 is preferentially enriched in dendrites in parallel with the expression and localization of MAP2 during the late stage of CGN polarization.

Depletion of MTCL2 resulted in the development of fewer and longer dendrites.

These results suggested the potential of MTCL2 to play an important role in the dendritic development of CGNs. To examine this possibility, we next examined the effects of MTCL2 knockdown in primary cultured CGNs. For this purpose, we transfected the plasmid expressing shRNA together with EGFP into CGNs 8 h after seeding. As shown in Fig. 2A, CGNs lacking MTCL2 exhibited apparently normal differentiation into neurons extending a long, thin axon. Quantification of axon length and branching did not reveal significant changes in MTCL2-depleted cells compared with control cells (Fig. 2B; Fig. S3A). In addition, MTCL2 depletion did not inhibit the appearance of MAP2-positive dendrites in DIV6 CGNs (Fig. 2C). However, detailed analyses revealed that MTCL2-depleted CGNs developed fewer dendrites than control cells in terms of the number of dendrite tips (Fig. 2D) and bases (Fig. S3B). On the other hand, the average length of the

dendrites of MTCL2-depleted CGNs (25.0 ± 11.5 μm) was larger than that of control cells (15.4 ± 4.00 μm) (Fig. 2E). The analysis of the length distribution of the dendrites of total CGNs indicated that the above increase in average length was mainly due to the existence of long dendrites in MTCL2-depleted cells, which were hardly observed in control cells (Fig. S3C). For example, the maximum dendritic length of individual CGNs was 35.7 ± 11.5 μm in average for control cells, but 54.0 ± 21.6 μm for MTCL2 knockdown cells (Fig. S3D). The proportion of dendrites longer than 40 μm in the total number of dendrites was 3.14 ± 0.13% in control cells, but 14.36 ± 0.10% in knockdown cells (Fig. 2F). The changes in dendrite numbers and length distribution observed in MTCL2-depleted cells were rescued by expressing RNAi-resistant mouse MTCL2 (Fig. 2D-F; Fig. S3B-D). Taken together, these results indicate that MTCL2 depletion results in aberrant CGN development with longer and fewer dendrites.

Dendrite extension and Golgi position are biased in the opposite direction to axon elongation in MTCL2-depleted CGNs

During the characterization of MTCL2-depleted CGNs, we noticed that their dendrite extension was biased in the direction opposite to axon elongation (see Fig. 2A,C). To confirm this tendency, we quantitatively estimated the direction of dendrite extension in the CGNs at DIV6. For this purpose, we measured angles based on the base positions of each dendrite (MAP2-positive neurite) and an axon (MAP2-negative, thin neurite) on the cell body (see illustration in Fig. 3A). Consistent with previous reports (Powell et al., 1997; Zmuda and Rivas, 1998), control cells extended dendrites in all directions evenly (Fig. 3B). On the other hand, their extension in MTCL2-depleted CGNs exhibited a strong bias toward the opposite and a slight bias toward the same direction of axon elongation when we focused on dendrites longer than 15 μm (Fig. 3B). The direction bias (r), defined as the ratio of dendrite numbers in the forward and backward directions and those in the left and right directions, were 1.22 ± 0.05 and 1.66 ± 0.10 for control and MTCL2-depleted cells, respectively (Fig. 3C). The expression of RNAi-resistant MTCL2 in MTCL2-depleted cells

suppressed this direction bias of dendritic extension to 1.01 ± 0.03 (Fig. 3B,C). These results indicate that MTCL2 depletion results in aberrant development of CGNs with longer and fewer bipolar dendrites (Fig. S3E).

Previous studies have demonstrated that the directions of neurite extension in cultured CGNs are closely coupled with the Golgi position in the cell body (Zmuda and Rivas, 1998). In the early stages of polarization, the Golgi apparatus was detected at the base of the initial or second process of unipolar or bipolar CGNs. However, they became random as cells became multipolar. Considering the fact that MTCL2 is a microtubule-crosslinking protein with the ability to bind the Golgi membrane, we next examined the possibility that MTCL2 knockdown affected the position of the Golgi apparatus in DIV6 CGNs (Fig. 3D-F). Again, we confirmed that the Golgi position was not biased to any direction in control CGNs, as reported previously (Zmuda and Rivas, 1998). However, in MTCL2-depleted CGNs, the Golgi position exhibited clear bias in the direction opposite to axon elongation, and was randomized again by the expression of RNAi-resistant MTCL2. Given the reported roles of the Golgi apparatus in dendrite development(Horton et al., 2005; Litterman et al., 2011; Puram and Bonni, 2013; Ye et al., 2007), these results suggest that MTCL2 depletion inhibits the multipolar extension of dendrites by suppressing the randomization of the Golgi position observed in mature CGNs.

MTCL2 is required for the bipolar-to-multipolar transition of dendrite extensions

Previous analyses of isolated cultures of CGNs have focused on the early stages of polarization when cells develop bipolar processes depending on the Golgi position (Powell et al., 1997; Zmuda and Rivas, 1998). However, there is limited information on how multipolar dendrites develop from initial bipolar CGNs (Kawaji et al., 2004; Kollins et al., 1999). Therefore, to reveal how MTCL2 inhibits the multipolar extension of dendrites, we next examined the polarity of dendrite extension in normal CGNs at the middle stage (DIV3), when cells should undergo the bipolar-to-multipolar transition (Fig. 4). The analysis demonstrated that dendrite extensions of DIV3 CGNs were clearly biased toward

the direction opposite to axon elongation, as observed in MTCL2-depleted cells (Fig. 4A,B, Fig. S4A). Furthermore, quantification of the dendrite lengths showed that the CGNs at DIV3 had longer dendrites than the CGNs at DIV5 (Fig. 4C, Fig. S4B). The positions of the Golgi apparatus in the CGNs at DIV3 were also clearly biased toward the direction of axon elongation (Fig. 4D, Fig. S4C). These results support the possibility that MTCL2 depletion inhibits the bipolar-to-multipolar transition of dendrite extension, which normally occurs between DIV3 and DIV5.

To directly examine this possibility, GFP-expressing CGNs at DIV3 with or without MTCL2 knockdown were subjected to live imaging, and their morphological changes were recorded every 2 min for 48 h (Fig. 4E,F). Consistent with the aforementioned results, cells extended bipolar neurites in addition to a thin long axon (arrowheads) at time 0 when recording began. The control cells elongated one thick neurite with a rather stable nature (arrow in Fig. 4E) and several short neurites showing dynamic growth and shrinkage in the opposite direction. However, a few hours after recording, the thick neurite began to shrink (6.2 ~ 9.2 h). In parallel, short neurites with a dynamic nature began elongating from various sites on the cell body (8.2h ~), and finally, the cell acquired a multipolar morphology with short dendrites (Fig. 4E; Fig. S4D; Movie 1). These results support the notion that the extension polarity of CGN's dendrites exhibited a bipolar-to-multipolar transition in which the length of the initial bipolar dendrites gradually decreases and new short dendrites appear in multiple directions in parallel. Most of the MTCL2-depleted CGNs exhibited shrinkage of the initial bipolar neurites (arrow) (13.2 ~ 17.2 h) and *de novo* elongation of unstable short dendrites (15.2 ~ 21.2 h) (Fig. 4F). However, they failed to steadily extend short dendrites longer than their cell body's width (~ 15μm) in multiple directions. Instead, MTCL2-depleted CGNs frequently elongated new long dendrites with stable nature along the initial bipolar axis (25.2 h ~) (Fig.4F; Fig. S4D; Movie 2). These results indicate that MTCL2 plays an indispensable role in the bipolar-to-multipolar transition of dendrite development in CGNs.

The Golgi-associating activity of MTCL2 is required for the multipolar elongation of

short dendrites but not the shrinkage of preexisting bipolar dendrites.

To explore how MTCL2 promotes the bipolar-to-multipolar transition of dendrite extension, we next examined the rescue activities of MTCL2 mutants lacking MT- (ΔKR) or Golgi- (4LA) binding activity in MTCL2-depleted CGNs (Fig. 2; Fig. 3; Fig. S3). In contrast to wild-type MTCL2, the ΔKR mutant did not rescue any defects in MTCL2 knockdown CGNs, including the reduced number and increased length of dendrites (Fig. 2D-F; Fig. S3B-D), and the biased polarity of dendrite elongation (Fig. 3B,C). These results indicate the crucial role of the MT-binding activity of MTCL2 in regulating dendrite development in CGNs. The 4LA mutant also failed to restore most of the defects, but interestingly, it exhibited substantial rescue activity solely for the length of dendrites (Fig. 2E,F, Fig. S3C,D). As a result, MTCL2 knockdown CGNs expressing RNAi-resistant MTCL2 4LA developed a reduced number of short dendrites with biased polarity (Fig. S3E).

The live imaging analysis in Fig. 4E revealed that the bipolar-to-multipolar transition of CGNs contained two events: the shrinkage of preexisting bipolar long neurites and the elongation of short, unstable neurites from multiple positions in the cell body. Therefore, the results of the knockdown/rescue experiments described above suggest that the two events observed in the bipolar-to-multipolar transition are differentially regulated by MTCL2, and the Golgi-binding activity of MTCL2 is required for the multidirectional development of short, unstable dendrites but not indispensable for the shortage of preexisting long neurites (Fig. S3E).

The Golgi apparatus extends upward along the microtubule cage surrounding the nuclei at the late stage of CGN polarization.

To understand how MTCL2 promotes the multipolar extension of *de novo* dendrites, we next examined the subcellular localization of MTCL2 in greater detail with respect to MTs.

Consistent with our previous observations in HeLa-K cells, basal confocal images of

matured CGNs (DIV5) revealed intermittent granular staining of MTCL2 on MT bundles running through MAP2-positive dendrites (Fig. S5A). In addition, many granular signals of MTCL2 were observed in the cell bodies (Fig. 5A; Fig. S5A). These signals frequently showed co-localization with an MT network, which was efficiently visualized by anti-tyrosinated but not anti-acetylated tubulin antibodies (Fig. S5B,C). A serial analysis of z stack confocal images (Fig. 5A,B) and their reconstructed views (Fig. 5C; Movie 3) revealed that such an MT network completely wraps the nucleus, indicating that it corresponds to the MT cage, the presence of which has been reported for CGNs (Rivas and Hatten, 1995; Solecki et al., 2004; Umeshima et al., 2007). Preferential staining using anti-tyrosinated but not anti-acetylated tubulin also supported this conclusion (Umeshima et al., 2007).

Surprisingly, in many CGNs at DIV5, the Golgi apparatus was associated with this MT cage at the lateral and apical surfaces of the nucleus (Fig. 5A). As a result, the Golgi apparatus extended its morphology toward the upward direction along the nuclear surface (Fig. 5C). In most extreme cases, it was completely placed on top of the nucleus (see arrows in Fig. 5C; Movie 3). This is completely different from the situation observed in CGNs at DIV2, where the Golgi apparatus was found at the basal position with biased localization to the base of one of the bipolar processes (Fig. 5D; Fig. S6A,B). At DIV2, some cells developed cortical MTs underneath the apical membranes of the cell bodies. However, they were not organized in a dense, isotropic network but tended to align parallel to the preexisting bipolar axis (Fig. 5D; Fig. S6A). Even at the CGNs at DIV3, where isotropic network-like MT structures were detected (Fig. S6A), the upward shift of the Golgi apparatus was not sufficiently observed (Fig. 5D; Fig. S6B). The quantitative analysis demonstrated that the cell heights did not differ significantly between CGNs at DIV3 and DIV5 (Fig. S7A,B). However, the height of the apical end of the Golgi apparatus relative to the corresponding cell height increased as the polarization proceeded (Fig. 5E). These results indicate that the final polarization process of CGNs is tightly coupled with the sequestration of the Golgi apparatus from the base of the bipolar neurites into the MT cage around the nuclei.

MTCL2 promotes the sequestering of the Golgi apparatus into the MT cage.

Importantly, in the CGNs at DIV5, many MTCL2 signals exhibited substantial overlap with those of the Golgi apparatus and MT signals around the nuclei (Fig. 5A-C). These results raise the intriguing possibility that MTCL2 plays an important role in the upward extension of the Golgi apparatus by mediating the association between the Golgi apparatus and the MT cage. To verify this possibility, we re-examined the Golgi positions in MTCL2-depleted cells in the z-direction. As expected, the Golgi positions in many MTCL2-depleted cells were significantly lowered (Fig. 6A). The quantitative analysis demonstrated that MTCL2 knockdown did not change the cell height (Fig. S7C). However, the apical ends of the Golgi apparatus were lowered to a similar level as those observed for bipolar CGNs at DIV3 (Fig. 6C). This defect was restored by expression of RNAi-resistant MTCL2 wild type, but not by MTCL2 ΔKR or 4LA (Fig. 6C). These results are consistent with the notion that MTCL2 promotes the upward extension of the Golgi apparatus along the nuclei by mediating the association between the Golgi apparatus and the MT cage.

In Fig. 3E and F, we demonstrate that MTCL2 knockdown suppresses the randomization of the Golgi position in the x-y plane observed in mature CGNs. We confirmed that neither the ΔKR nor 4LA mutant restored this random distribution of the Golgi apparatus in MTCL2-depleted cells (Fig. 3D-F). These results indicate that changes in the Golgi position within the x-y plane and in the z-direction were tightly coupled and simultaneously induced, probably by the MTCL2-mediated sequestration of the Golgi apparatus into the MT cage (Fig. 7A).

LINC complex activity is required for the sequestering of the Golgi apparatus into the MT cage.

It is not clear how the MT cage develops around the nuclei. However, the involvement of the LINC complex was strongly suspected because it provides a linkage between the

nuclear membrane and MTs via MT motors (Fig. 7A, right) (Chang et al., 2015; Kengaku, 2018). In addition, recent studies have revealed the indispensable roles of the LINC complex in nuclear rotation, deformation, and translocation during CGN migration (Wu et al., 2018; Zhou et al., 2024). Therefore, to validate the important roles of the MT cage in the bipolar-to-multipolar transition of dendrite extension, we next examined the role of the LINC complex by inhibiting its function.

One component of the LINC complex is outer nuclear membrane proteins such as nesprin1 and 2, which interact with MT motors through N-terminal cytoplasmic stretch (Fig. 7A, right), and the other is the inner nuclear membrane proteins, the SUN proteins, which interact with the nuclear lamina and chromatins within nuclei (Fig. 7A, right). Nesprins interact with SUN proteins through its C-terminal KASH domains within perinuclear space (Fig. 7A, right), and the expression of the nesprin-1 mutant lacking the N-terminal stretch (KASH1) inhibits LINC complex activity by dominantly interfering with the interaction between endogenous nesprins and SUN proteins (Stewart-Hutchinson et al., 2008; Wu et al., 2018).

When GFP-KASH1 was expressed in primary cultured CGNs, its localization to the nuclear membrane was detected as expected (Fig. 7B). Close inspections revealed network-like distributions of GFP-KASH1 that likely reflect the nuclear lamina pattern underneath the inner nuclear membrane via SUN proteins (Fig. 7C; Fig. S8A). In these GFP-KASH1–expressing cells, but not GFP-expressing cells, the randomization of the Golgi position in a x-y plane (Fig. 7D, Fig. S8B) and the upward extension of the Golgi apparatus in the z direction (Fig. 7B,E) were suppressed, as observed in MTCL2-depleted CGNs. Because GFP-KASH1 expression did not affect the colocalization of MTCL2 with the Golgi apparatus and MT cage (Fig. 7B,C; Fig. S8A), these results suggest that the normal function of the LINC complex plays an important role in changing the Golgi position both in x-y plane and in the z direction, independent of the MTCL2 function.

Importantly, when the dendrite extension polarity was examined, cells expressing GFP-KASH1 exhibited a reduced number of dendrites with a biased extension direction to the preexisting bipolar axis (Fig. 7F,G; Fig. S8C). Because these cells did not show significant

reductions in dendritic length (Fig. 7H; Fig. S8D), they perfectly mimicked the phenotypes exhibited by MTCL2-depleted CGNs expressing the MTCL2 mutant lacking Golgi-binding activity (Fig. S3E, Fig. S8E). These results support our proposal that the sequestering of the Golgi apparatus to the MT cage is important for the multipolar development of short, unstable dendrites observed in CGNs at the final stage of their polarization.

Discussion

Previously, we characterized MTCL2 as a unique MT-regulating protein with Golgi-binding activity (Matsuoka et al., 2022). Here, we demonstrate that MTCL2 is highly expressed in CGNs and plays an indispensable role in the later stage of polarization when dendrite extensions undergo a bipolar-to-multipolar transition. We provide evidence suggesting that MTCL2 facilitates this transition by mediating the interaction between the Golgi apparatus and the MT cage surrounding the nuclei, which liberates the Golgi apparatus from preexisting bipolar dendrites and enables it to function in multipolar extensions of *de novo* dendrites.

The unique polarization process observed in isolated CGN cultures was first reported in 1997 (Powell et al., 1997). Subsequent studies by the same groups have established that CGNs have an intrinsic program for monopolar and bipolar morphology before developing their final morphology with multipolar short dendrites (Kollins et al., 1999; Zmuda and Rivas, 1998). The importance of Golgi apparatus positioning in disrupting initial bipolarity was also implicated in these early studies(Zmuda and Rivas, 1998). However, due to the limitations of subsequent studies that extended these pioneering works, particularly those that performed live-imaging analysis (Kawaji et al., 2004; Kollins et al., 1999), many aspects of the polarization process of CGNs remain to be clarified. An important question is how the initial bipolarity transforms into the final complex morphology of multipolar dendrites. In this paper, we focused on this issue and demonstrated for the first time that the initial extensions of multiple dendrites are still affected by preexisting bipolarity (Fig.4). The live imaging analysis of CGNs from DIV3 to DIV5 not only supported this conclusion but further revealed that this bipolar-to-multipolar transition of dendrite extension constitutes two distinct processes: destabilization of preexisting bipolar dendrites to make them shorter, and the *de novo* generation of unstable dendrites from the multiple sites of the cell body (Fig. 4E,F). MTCL2 knockdown inhibited both processes, resulting in fewer and longer dendrites with the extension bias to the opposite direction to an axon (Fig 3A-C). Interestingly, the rescue experiments suggested that the MT-binding activity of MTCL2 is

required for both processes, whereas the Golgi-binding activity is dispensable for the destabilization of the preexisting bipolar dendrites and only required for the *de novo* generation of multipolar dendrites from the cell body.

It is unknown why the MT-binding activity of MTCL2 contributes to the destabilization of bipolar dendrites. However, we succeeded in providing data indicating how MTCL2 promotes the multipolar development of *de novo* dendrites through its MT- and Golgi-binding activities. Based on our novel findings on the MTCL2-dependent upward extension of the Golgi apparatus along the nuclei (Fig. 5), we propose the working hypothesis that MTCL2 mediates the association between the Golgi apparatus and the MT cage, thus promoting sequestering of the Golgi apparatus from the base of preexisting bipolar dendrites (Fig. 7A). Importantly, the upward extension of the Golgi apparatus was tightly coupled with the randomization of the Golgi position (Fig. 7A). Therefore, we further propose that the sequestering of the Golgi apparatus to the MT cage not only suppresses dendrite elongation along the preexisting bipolar axis and enables the Golgi apparatus to move randomly around the nuclei and work for dendritic extension in multiple directions.

Here, we demonstrate that the upward extension of the Golgi membrane requires the normal formation of a LINC complex (Chang et al., 2015). Because GFP-KASH1 expression disrupts the LINC complex-mediated fixation of MT motors to the nuclear lamina (Stewart-Hutchinson et al., 2008), our results suggest that the pulling forces generated by MT motors play a role in attracting the Golgi apparatus to the MT cage and inducing its upward extension. Considering recent studies demonstrating that the LINC complex plays an indispensable role in the MT motor-dependent nuclear rotation required for the migration of bipolar CGNs (Wu et al., 2018; Zhou et al., 2024), the LINC complex might also contribute to the random positioning of the Golgi apparatus around the nuclei observed in mature CGNs.

Taken together, the results of this study provide clues to answer the long-standing question: how do neurons disrupt bipolarity to extend dendrites into multiple directions. Our results highlight the importance of the MT cage surrounding the nuclei in randomizing the Golgi positions required for the multipolar extension of dendrites. The critical

importance of the MTCL2-mediated association between the Golgi apparatus and the MT cage, as well as that of the LINC complex-mediated fixation of MT motors to the nuclear membrane, was also suggested, although the underlying molecular mechanisms should be further clarified in future studies.

Materials and Methods

Animals

All protocols were approved by and performed in accordance with the guidelines established by the Institutional Animal Care and Use Committee of Yokohama City University, Medical Life Science (Approval No. T-A-19-006 and T-A-22-007).

Antibodies

The primary antibodies used in this study were as follows: anti-SOGA1 to detect MTCL2 (HPA043992), anti-tau1 (MAB3420), anti-calbindin (C9848) from Sigma-Aldrich ; anti-MAP2 (sc-32791), anti-α-tubulin (DM1A: sc-32293), anti-acetylated tubulin (sc-23950), anti-tyrosinated tubulin (sc-53029), anti-GFP (sc-9996) from Santa Cruz Biotechnology; anti-GM130 (610822) and anti-GS28 (611184) from BD Transduction Laboratories; anti-GAPDH (5G4) from HyTest Ltd; and anti-NeuN (MAB377) from Merck Millipore.

Primary Neuron Culture and Transfection

Primary cerebellar granule neurons (CGNs) were isolated from P6 neonatal mice and prepared as previously described (Krämer and Minichiello, 2010). Neurons were plated on coverslips coated with poly-D-lysin (0.1 mg/mL; Sigma or Thermo Fisher) at a density of 180,000 cells/well, 300,000 cells/well, or 360,000 cells/well (24 well plates) and cultured for 8 h in Dulbecco's modified Eagle medium (DMEM) (Life Technologies Corporation) containing 10% fetal bovine serum, penicillin (100 U/ml), streptomycin (0.1 mg/ml), 3.5 mM glutamine, and 0.9 mM sodium pyruvate (nacalai) under controlled temperature and CO_2 conditions (37°C, 5%). Then, cells were subjected to plasmid transfection using a CalPhos^T Mammalian Transfection Kit (Takara) according to the manufacturer's instruction for 8~16 h, followed by incubation with the original medium supplemented with 0.01 mM Ara-C (Tokyo Chemical Industry Co., Ltd.) and 20 mM KCl until fixation.

Plasmids

For knockdown experiments, pEB-super-GFP vectors simultaneously expressing EGFP and appropriate shRNA were first constructed (Masuda-Hirata et al., 2009). Then, the EBNA1 cDNA sequence and the associated CMV promoter were removed to reduce vector size. For mouse MTCL2 knockdown, the RNAi target sequence 5′-gacggtcagtgtaggtcttca-3′ was inserted under the H1 promoter as a hairpin oligonucleotide sequence in a tail-to-tail fashion (Satake et al., 2017). The control shRNA sequence used was 5′-cagtcgcgtttgcgactgg-3′. To generate RNAi-resistant mouse MTCL2 expression vectors, silent mutations (a act gta tca gtc ggc ttg cag a) in the RNAi target sequence were introduced in the cDNAs of V5-tagged wild-type or mutant mouse MTCL2 (4LA or ΔKR) subcloned in the pCAGGS expression vector (Matsuoka et al., 2022). In rescue experiments, the shRNA expression vector for mouse MTCL2 and appropriate expression vectors for RNA-resistant mouse MTCL2 wild type or mutant MTCL2 were co-transfected into CGNs. To construct a GFP-KASH1 expression vector, a human nesprin-1 cDNA fragment encoding the C-terminal region (8726-8799 a.a.) was amplified by RT-PCR from total RNA from HeLa-K cells and cloned into pEGFP-C1 at GglI/BamHI sites (Stewart-Hutchinson et al., 2008). The resulting GFP-KASH1 cDNA fragment was subcloned into the pCAGGS vector to change the promoter.

Immunocytochemistry

The CGNs were fixed in 4% paraformaldehyde (PFA) at room temperature for 15 min at 37°C. After fixation and blocking, samples were incubated with appropriate primary antibodies diluted in TBST (10 mM Tris–HCl pH 7.5, 150 mM NaCl, 0.01% [v/v] Tween 20) containing 0.1% (w/v) BSA overnight at 4 °C. After washing with PBST, samples were incubated with the appropriate secondary antibodies conjugated with Alexa Fluor 488, 555, or 647 (Life Technologies Corporation) for 60 min at room temperature. Dilutions of the used antibodies are as follows: anti-SOGA1 (1/2000), anti-α-tubulin (1:1000), anti-acetylated tubulin (1:1000), anti-tyrosinated tubulin (1:4000), anti-GM130 (1:1000), anti-GS28 (1:300), anti-GFP (1:2,000), anti-MAP2 (1:1000), and anti-tau1 (1:1000). All secondary antibodies were used at a 1:2000 dilution. The nuclei were counterstained with 4',

6-diamidino-2-phenylindole (MBL, Japan) at a 1:2000 dilution in PBST during the final wash. For image acquisition, samples on coverslips were mounted onto glass slides in Prolong Diamond Antifade Mountant (Thermo Fisher Scientific).

Immunohistochemistry

Mice under deep isoflurane anesthesia were fixed by transcardial perfusion with 4% paraformaldehyde (PFA) in 0.1 M PB (0.1 M NaH2PO4 and 0.1 M Na2HPO4, pH 7.4). Brains were removed from the skull, post-fixed for 3–5 h at room temperature, and sectioned at 50-µm thickness using a Vibratome (VT1200S; Leica Microsystems, Wetzlar, Germany). Following permeabilization with 0.1% Triton-X-100 in 0.1 M PB with gentle shaking for 30 min, cerebellar vermis slices were blocked with 10% calf serum in TBST for 30 min at room temperature. Immunofluorescence staining was performed as previously described.

Image acquisition and processing

Most images were acquired using a Leica SP8 laser scanning confocal microscope equipped with an HC PL APO 63x/1.40 Oil 2 objective using the Hybrid Detector in photon-counting mode. To obtain super-resolution images, HyVolution2 imaging was performed on the same system using Huygens Essential software (Scientific Volume Imaging). Single confocal images are shown unless otherwise indicated. The same confocal system was used to obtain time-lapse images, except that an HC PL APO 20x/0.75 objective was used. Cells seeded onto 35-mm glass-bottom dishes and subjected to appropriate transfection were placed in a closed heat-controlled chamber (Leica) with a CO2 supply system (Tokken) on the microscope stage for 2 days under autofocus control. Wide-view or low-resolution images for quantification (Figs. 2, 3, and 4) were obtained using an AxioImager ZI microscope (Carl Zeiss, Oberkochen, Germany) equipped with a Plan-Apochromat 40×/0.95 objective and an Orca II CCD camera (Hamamatsu Photonics, Shizuoka, Japan). To obtain images of brain slices and to measure the heights of cells and the apical end of the Golgi apparatus, an AxioImager Z1 microscope equipped with a

CSU10 disc confocal system (Yokogawa Electric Corporation, Tokyo, Japan) and a 20x/1.4 NA or 100x/1.46 NA Plan-apochromat objective was used. Images were acquired using MetaMorph software (Molecular Devices, Sunnyvale, CA) and processed using ImageJ software to obtain appropriate brightness and contrast.

Quantification

To quantify the enrichment of MTCL2 and MAP2 in CGN neurites, immunofluorescence signal intensities of anit-MTCL2 and anti-MAP2 staining were measured in ROIs of 1 μm^2 circles placed on anti-acetylated tubulin- or tau1-positive neurites. To analyze the morphology of CGNs, the positions of bases, tips, or branching points of neurites (axons or dendrites) were marked manually, and their lengths and numbers of tips were automatically quantified using the NeuronJ plugin for ImageJ. Essential functions of ImageJ were used to manually analyze the polarity of the dendrite extension direction, Golgi position in the x–y plane, and number of bases of dendrites. The dendritic lengths of CGNs subjected to live imaging were also analyzed manually. The cell height and position of the Golgi apical end were determined from the focal plane at which the fluorescent signals of tyrosinated tubulin and GS28 were disappeared in z-stack images taken at an interval of 0.3 μm. The 3D video shown in Movie 3 was created using a software (LAS X) associated with the Leica SP8 laser scanning confocal system.

Cell extraction and western blotting

CGN extracts were prepared by adding RIPA buffer (25 mM Tris/HCl [pH 7.5], 150 mM NaCl, 1% NP40, 1% deoxycholic acid, 0.1% SDS) containing a protease inhibitor cocktail (Sigma-Aldrich, P8340), followed by brief sonication and centrifugation (15,000 × *g*, 15 min). Samples were separated using SDS-PAGE and transferred to polyvinylidene fluoride membranes. Blots were incubated in blocking buffer containing 5% (w/v) dried skim milk in PBST (8.1 mM $Na_2HPO_4.12H_2O$, 1.47 mM KH_2PO_4, 137 mM NaCl, 2.7 mM KCl, and 0.05% Tween 20), followed by overnight incubation with anti-SOGA1 or anti-GAPDH antibodies diluted in blocking buffer. The diluted anti-SOGA1 and anti-GAPDH antibodies

were 1:1000 and 1:5000, respectively. Blots were then exposed to horseradish peroxidase (HRP)-conjugated secondary antibodies (GE Healthcare) diluted in blocking buffer for 60 min at room temperature and washed again. Blots were visualized using an Immobilon Western Chemiluminescent HRP Substrate (Millipore) or ECL western blotting detection system (GE Healthcare). Chemiluminescence was quantified using an ImageQuant LAS4000 Luminescent Image Analyzer (GE Healthcare).

Acknowledgments

We thank Dr. Tomoko Satake for her initial support in the establishment of the primary cerebellar granule cell culture.

Competing interests

No competing interests were declared.

Funding

This research was supported by KAKENHI (to A.S.) (Grant Numbers 19H03228 and 22H02621) of the Ministry of Education, Culture, Sports, Science and Technology (MEXT) of Japan.

Author contributions

Conceptualization: A.S.; Methodology: A.S, M.M.; Validation: M.M.; Formal analysis: M.M.; Investigation: A.S, M.M.; Resources: A.S, M.M.; Data curation: A.S, M.M.; Writing: A.S.; Supervision: A.S.; Funding acquisition: A.S.

Conflict of interest

The authors declare no conflicts of interest.

References

Arakawa, Y., Bito, H., Furuyashiki, T., Tsuji, T., Takemoto-Kimura, S., Kimura, K., Nozaki, K., Hashimoto, N. and Narumiya, S. (2003). Control of axon elongation via an SDF-1α/Rho/mDia pathway in cultured cerebellar granule neurons. *Journal of Cell Biology* 161, 381–391.

Chang, W., Worman, H. J. and Gundersen, G. G. (2015). Accessorizing and anchoring the LINC complex for multifunctionality. *J Cell Biol* 208, 11–22.

Dotti, C. G., Sullivan, C. A. and Banker, G. A. (1988). The establishment of polarity by hippocampal neurons in culture. *J Neurosci* 8, 1454–1468.

Fletcher, T. L. and Banker, G. A. (1989). The establishment of polarity by hippocampal neurons: The relationship between the stage of a cell's development in situ and its subsequent development in culture. *Dev Biol* 136, 446–454.

Hatten, M. E. and Heintz, N. (1995). Mechanisms of Neural Patterning and Specification in the Development Cerebellum. *https://doi.org/10.1146/annurev.ne.18.030195.002125* 18, 385–408.

Horton, A. C., Rácz, B., Monson, E. E., Lin, A. L., Weinberg, R. J. and Ehlers, M. D. (2005). Polarized secretory trafficking directs cargo for asymmetric dendrite growth and morphogenesis. *Neuron* 48, 757–771.

Huang, J., Furuya, A. and Furuichi, T. (2007). Very-KIND, a KIND domain containing RasGEF, controls dendrite growth by linking Ras small GTPases and MAP2. *J Cell Biol* 179, 539–552.

Kawaji, K., Umeshima, H., Eiraku, M., Hirano, T. and Kengaku, M. (2004). Dual phases of migration of cerebellar granule cells guided by axonal and dendritic leading processes. *Molecular and Cellular Neuroscience* 25, 228–240.

Kengaku, M. (2018). Cytoskeletal control of nuclear migration in neurons and non-neuronal cells. *Proc Jpn Acad Ser B Phys Biol Sci* 94, 337–349.

Kitazawa, A., Kubo, K. I., Hayashi, K., Matsunaga, Y., Ishii, K. and Nakajima, K. (2014). Hippocampal pyramidal neurons switch from a multipolar migration mode to a novel

"climbing" migration mode during development. *Journal of Neuroscience* 34, 1115–1126.

Kollins, K. M., Powell, S. K. and Rivas, R. J. (1999). GPI-anchored human placental alkaline phosphatase has a nonpolarized distribution on the cell surface of mouse cerebellar granule neurons in vitro. *J Neurobiol* 39, 119–141.

Krämer, D. and Minichiello, L. (2010). Cell culture of primary cerebellar granule cells. *Methods Mol Biol* 633, 233–239.

Litterman, N., Ikeuchi, Y., Gallardo, G., O'Connell, B. C., Sowa, M. E., Gygi, S. P., Harper, J. W. and Bonni, A. (2011). An OBSL1-CUl7Fbxw8 ubiquitin ligase signaling mechanism regulates golgi morphology and dendrite patterning. *PLoS Biol* 9, 17–19.

Mandell, J. W. and Banker, G. A. (1996). A spatial gradient of tau protein phosphorylation in nascent axons. *Journal of Neuroscience* 16, 5727–5740.

Masuda-Hirata, M., Suzuki, A., Amano, Y., Yamashita, K., Ide, M., Yamanaka, T., Sakai, M., Imamura, M. and Ohno, S. (2009). Intracellular polarity protein PAR-1 regulates extracellular laminin assembly by regulating the dystroglycan complex. *Genes to Cells* 14, 835–850.

Matsuoka, R., Miki, M., Mizuno, S., Ito, Y., Yamada, C. and Suzuki, A. (2022). MTCL2 promotes asymmetric microtubule organization by crosslinking microtubules on the Golgi membrane. *J Cell Sci* 135,.

Millen, K. J., Wurst, W., Herrup, K. and Joyner, A. L. (1994). Abnormal embryonic cerebellar development and patterning of postnatal foliation in two mouse Engrailed-2 mutants. *Development* 120, 695–706.

Miyata, T., Kawaguchi, A., Saito, K., Kawano, M., Muto, T. and Ogawa, M. (2004). Asymmetric production of surface-dividing and non-surface-dividing cortical progenitor cells. *Development* 131, 3133–3145.

Nagata, I. and Nakatsuji, N. (1990). Granule cell behavior on laminin in cerebellar microexplant cultures. *Developmental Brain Research* 52, 63–73.

Noctor, S. C., Martinez-Cerdeño, V., Ivic, L. and Kriegstein, A. R. (2004). Cortical neurons arise in symmetric and asymmetric division zones and migrate through specific phases. *Nature Neuroscience 2004 7:2* 7, 136–144.

Oishi, Y., Hashimoto, K., Abe, A., Kuroda, M., Fujii, A. and Miyamoto, Y. (2021). Vitronectin regulates the axon specification of mouse cerebellar granule cell precursors via αvβ5 integrin in the differentiation stage. *Neurosci Lett* 746, 135648.

Powell, S. K., Rivas, R. J., Rodriguez-Boulan, E. and Hatten, M. E. (1997). Development of polarity in cerebellar granule neurons. *J Neurobiol* 32, 223–236.

Puram, S. V. and Bonni, A. (2013). Cell-intrinsic drivers of dendrite morphogenesis. *Development (Cambridge)* 140, 4657–4671.

Rao, A. N., Falnikar, A., O'Toole, E. T., Morphew, M. K., Hoenger, A., Davidson, M. W., Yuan, X. and Baas, P. W. (2016). Sliding of centrosome-unattached microtubules defines key features of neuronal phenotype. *Journal of Cell Biology* 213, 329–341.

Rivas, R. J. and Hatten, M. E. (1995). Motility and cytoskeletal organization of migrating cerebellar granule neurons. *Journal of Neuroscience* 15, 981–989.

Satake, T., Yamashita, K., Hayashi, K., Miyatake, S., Tamura-Nakano, M., Doi, H., Furuta, Y., Shioi, G., Miura, E., Takeo, Y. H., et al. (2017). MTCL1 plays an essential role in maintaining Purkinje neuron axon initial segment. *EMBO J* 36, 1227–1242.

Solecki, D. J., Model, L., Gaetz, J., Kapoor, T. M. and Hatten, M. E. (2004). Par6α signaling controls glial-guided neuronal migration. *Nat Neurosci* 7, 1195–1203.

Solecki, D. J., Govek, E. E., Tomoda, T. and Hatten, M. E. (2006). Neuronal polarity in CNS development. *Genes Dev* 20, 2639–2647.

Stewart-Hutchinson, P. J., Hale, C. M., Wirtz, D. and Hodzic, D. (2008). Structural requirements for the assembly of LINC complexes and their function in cellular mechanical stiffness. *Exp Cell Res* 314, 1892–1905.

Tahirovic, S. and Bradke, F. (2009). Neuronal polarity. *Cold Spring Harb Perspect Biol* 1, 1–18.

Takano, T., Xu, C., Funahashi, Y., Namba, T. and Kaibuchi, K. (2015). Neuronal polarization. *Development (Cambridge)* 142, 2088–2093.

Tan, M., Ma, S., Huang, Q., Hu, K., Song, B. and Li, M. (2013). GSK-3α/β-mediated phosphorylation of CRMP-2 regulates activity-dependent dendritic growth. *J Neurochem* 125, 685–697.

Umeshima, H., Hirano, T. and Kengaku, M. (2007). Microtubule-based nuclear movement occurs independently of centrosome positioning in migrating neurons. *Proc Natl Acad Sci U S A* 104, 16182–16187.

Witte, H., Neukirchen, D. and Bradke, F. (2008). Microtubule stabilization specifies initial neuronal polarization. *Journal of Cell Biology* 180, 619–632.

Wu, Y. K., Umeshima, H., Kurisu, J. and Kengaku, M. (2018). Nesprins and opposing microtubule motors generate a point force that drives directional nuclear motion in migrating neurons. *Development* 145,.

Ye, B., Zhang, Y., Song, W., Younger, S. H., Jan, L. Y. and Jan, Y. N. (2007). Growing Dendrites and Axons Differ in Their Reliance on the Secretory Pathway. *Cell* 130, 717–729.

Zhou, C., Wu, Y. K., Ishidate, F., Fujiwara, T. K. and Kengaku, M. (2024). Nesprin-2 coordinates opposing microtubule motors during nuclear migration in neurons. *J Cell Biol* 223,.

Zmuda, J. F. and Rivas, R. J. (1998). The Golgi Apparatus and the Centrosome Are Localized to the Sites of Newly Emerging Axons in Cerebellar Granule Neurons In Vitro. *Cell Motil Cytoskeleton* 41, 18–38.

Figure Legends

Figure 1. MTCL2 is preferentially enriched in the dendrites of cerebellar granule neurons.

(A) Cerebellar sections from 4-week-old mice are stained for calbindin and NeuN (left panel) or MTCL2 and α-tubulin (middle and right panels). Scale bars: 250 μm. (B) Representative images of isolated CGNs cultured for 5 days and stained for acetylated tubulin, MTCL2, and MAP2. Scale bar: 20 μm. (C) Correlation between the immunofluorescence intensities of MTCL2 and MAP2 in acetylated tubulin-positive neurites. A total of 100 neurites from 3 independent experiments were analyzed. (D) Representative images of CGNs at DIV1–DIV5 stained for tau1, MTCL2, and MAP2. In the merged view, nuclei staining is included to clarify the positions of cell bodies. The arrowheads indicate tau1-positive neurites exhibiting MTCL2 signals in immature CGNs. Scale bar: 20 μm. (E) Time-dependent increase in the relative intensities of the MTCL2 (blue bars) and MAP2 (green bars) signals in dendrites and their correlation (dotted line). Neurites exhibiting MAP2 signal intensities three times greater than the background were analyzed as dendrites. Data represent the means ± S.E. from 3 independent experiments (totally, more than 67 neurites were analyzed for each DIV stage). The paired t-test was used to examine statistical significance (**$p < 0.01$; ***$p < 0.005$; n.s., non-significant). (F) Western blot analysis of MTCL2 and MAP2 expression in primary cultured CGNs from various DIVs. A representative result of 2 independent experiments is presented.

Figure 2. Depletion of MTCL2 resulted in the development of fewer and longer dendrites.

(A) Full views of single CGNs at DIV6 visualized by the GFP signal. Scale bar: 50 μm. (B) Distribution of total axonal length of individual CGNs subjected to the indicated RNAi and fixed at DIV6. (C) Dendritic development of DIV6 CGNs transfected with control or MTCL2 knockdown vectors and visualized by GFP and MAP2 signals. The arrowheads indicate the dendrites of GFP-positive cells. Scale bar: 10 μm. (D) Distribution of total

number of dendritic tips of individual CGNs subjected to the indicated RNAi/rescue conditions and fixed at DIV6. (E) Distribution of averaged dendritic lengths of the individual CGNs analyzed in (D). (F) Percentage of dendrites longer than 40 μm in all dendrites of the same CGNs analyzed in (D) and (E). Each data point in (B), (D), and (E) represents the result of one neuron in 3 independent experiments. Mean values and standard deviations are shown for each scatter plot. The bars in (F) represent mean values and standard errors of 3 independent experiments. For all data, the paired t-test was used to examine statistical significance (*$p < 0.05$; **$p < 0.01$; ***$p < 0.005$; n.s., non-significant).

Figure 3. Dendrite extensions and Golgi apparatus positions of MTCL2-depleted CGNs biased in the direction opposite to axonal elongation.

(A) The extension directions of dendrites longer than 15 μm were defined as the angle (θ) formed between the roots of the dendrite and an axon, as depicted. (B) θ distribution of individual dendrites of CGNs subjected to the indicated RNAi/rescue conditions and fixed at DIV6. The θ values were categorized in 4 directions and presented in polar histograms as indicated. More than 350 dendrites from the indicated number (n) of cells from 3 independent experiments were analyzed for each condition. (C) Comparison of dendritic direction bias (r) between the conditions. r =1 indicates no direction bias. (D) The position of the Golgi apparatus for individual CGNs was estimated as the angle (θ) formed between the center of the Golgi apparatus and the roots of an axon, as depicted. (E) θ distribution of the Golgi position in CGNs subjected to the indicated RNAi/rescue conditions and fixed at DIV6. The θ values were categorized in 4 directions and presented in polar histograms as indicated. The numbers (n) of cells from 3 independent experiments were analyzed. (F) Comparison of direction bias (r) of the Golgi position under each condition. Mean values and standard errors are shown for all quantitative data for each condition. In (C) and (F), the paired t-test was used to examine statistical significance (*$p < 0.05$; ***$p < 0.005$; n.s., non-significant).

Figure 4. MTCL2 is required for the bipolar-to-multipolar dendrite extension

transition.

(A) Representative morphologies of CGNs at DIV3 and DIV5 visualized by GFP. Arrowheads indicate axons. Scale bar: 20 μm. (B) θ distribution of individual dendrites of CGNs at DIV3 and 5. Data are presented as polar histograms for >350 dendrites of the indicated number (n) of cells from 3 independent experiments for each condition, as in Fig. 3B. (C) Distribution of the average dendritic length of individual CGNs analyzed in (B). Each data point represents the result of one neuron in 3 independent experiments. Mean values and standard deviations are shown for each scatter plot. (D) Comparison of the direction bias (r) of the Golgi position in the GCNs at DIV3 and DIV5. The mean values and standard errors of 3 independent experiments are shown for each condition. In (C) and (D), the paired t test was used to examine statistical significance (*$p < 0.05$; ***$p < 0.005$). (E, F) Representative live imaging data of GFP-expressing CGNs transfected with control (E) or MTCL2 (F) knockdown vectors. In each case, bipolar CGNs were selected at DIV3, and recordings were performed for 48 h. Frames showing the characteristic changes in the dendrite extensions are presented for each CGN. Arrowheads indicate axons. Arrows indicate initial stable dendrites. Note that the MTCL2-depleted CGN exhibited shrinkage of the preexisting bipolar dendrites but failed to stably extend short dendrites in multiple directions. Instead, the cell stably extended long bipolar dendrites, again. Scale bars: 50 μm.

Figure 5. The Golgi apparatus in the differentiated CGNs was sequestered into the MT cage surrounding the nuclei.

(A) High-resolution confocal images of mature CGNs (DIV5) stained for tyrosinated tubulin, MTCL2, and GS28 (Golgi membrane protein). Three images of the same field in different confocal planes are presented from the basal to apical planes, as indicated. Scale bar: 5 μm. (B) Boxed regions in (A) were enlarged to show substantial colocalization of tyrosinated tubulin, MTCL2, and the Golgi apparatus. Scale bar: 5 μm. (C) Cross-sectional views of the z-stack images along the dotted line in (A). Two types of merged images with different antibody combinations are presented. The arrows indicate the Golgi apparatus at the top of the nucleus. Scale bar: 2 μm. (D) High-resolution confocal images of immature

CGNs at DIV2 and DIV3 after staining with tyrosinated tubulin and GS28. Scale bar: 5 μm. (E) Height distribution of the apical edge of the Golgi apparatus estimated as a percentage of the cell heights (see Fig. S7). Each data point represents the result of one neuron observed in 3 independent experiments. Mean values and standard deviations are shown for each scatter plot. The paired t-test was used to examine statistical significance (**$p < 0.01$; ***$p < 0.005$).

Figure 6. MTCL2 promotes the upward extension of the Golgi apparatus in an MT- and Golgi-binding activity-dependent manner.

(A) High-resolution confocal images of CGNs subjected to the indicated RNAi, fixed at DIV6, and stained for tyrosinated tubulin and GS28. On the left, projected views of the z-stack images indicate cells expressing the indicated shRNA vector together with GFP. Images obtained at three different confocal planes are shown on the right. Scale bar: 5 μm. (B) Cross-sectional views of the z-stack images along the dotted lines in (A). Asterisks indicate GFP-positive cells. Scale bar: 5 μm. (C) Height distribution of the Golgi apical edge in CGNs subjected to the indicated RNAi/rescue conditions and fixed at DIV6. Each data point represents the result of one neuron observed in 3 independent experiments. Mean values and standard deviations are shown for each scatter plot. The paired t-test was used to examine statistical significance (***$p < 0.005$; n.s., non-significant).

Figure 7. Inhibition of LINC complex activity mimicked most of the phenotypes shown by MTCL2 knockdown.

(A) Schematic illustration of our working hypothesis. At the late phase of CGN polarization, the MTCL2-mediated association between the Golgi apparatus and the MT cage induces an upward extension of the Golgi apparatus along the nuclei. This recruitment to the MT cage not only sequesters the Golgi apparatus from the root of the preexisting bipolar dendrites but also enables it to move randomly around the nuclei, finally promoting the multipolar extension of short dendrites. On the right, the molecular organization of the LINC complex on the nuclear membrane is illustrated. (B) A typical cross-sectional view of

CGNs expressing GFP-KASH1, fixed at DIV6, and stained for MTCL2 and GS28. The white dotted lines indicate the focus plane from which the confocal image shown in Fig. S8A was obtained. Scale bar: 5 μm. (C) An apical confocal section of a GFP-KASH1-expressing cell stained for MTCL2 and tyrosinated tubulin. Scale bar: 5 μm.(D) θ distribution of the Golgi position in CGNs expressing GFP or GFP-KASH1, examined at DIV6. Data are presented as polar histograms as shown in Fig. 3E for the indicated number (n) of cells from 3 independent experiments. (E) Hight distribution of the Golgi apical edge in the same CGNs analyzed in (C). (F) θ distribution of individual dendrites of CGNs expressing GFP or GFP-KASH1 and examined at DIV6. Data are presented as polar histograms in Fig. 3B for >400 dendrites of the indicated number (n) of cells from 3 independent experiments. (G, H) Distribution of the number of dendritic tips (G) and averaged dendritic length (H) of the same CGNs analyzed in (F). Each data point in (E), (G) and (H) represents the result of a single neuron. Mean values and standard deviations are shown for each scatter plot. The paired t-test was used to examine statistical significance (***$p < 0.005$; n.s., non-significant).

Movie Legends

Movie 1. Morphological changes in the control CGN from DIV3 to DIV5.

GFP fluorescence images were taken every 2 min for 40 h. The video speed was 30 fps. The representative frames of this movie are shown in Fig. 4E.

Movie 2. Morphological changes in the MTCL2-depleted CGN from DIV3 to DIV5.

GFP fluorescence images were taken every 2 min for 40 h. The video speed was 30 fps. The representative frames of this movie are shown in Fig. 4F.

Movie 3. 3D reconstructed images of polarized CGNs at DIV5.

The z-stack images of the CGNs shown in Fig. 5A were reconstructed into 3D stereoscopic images with different combinations of staining.

Figure 1

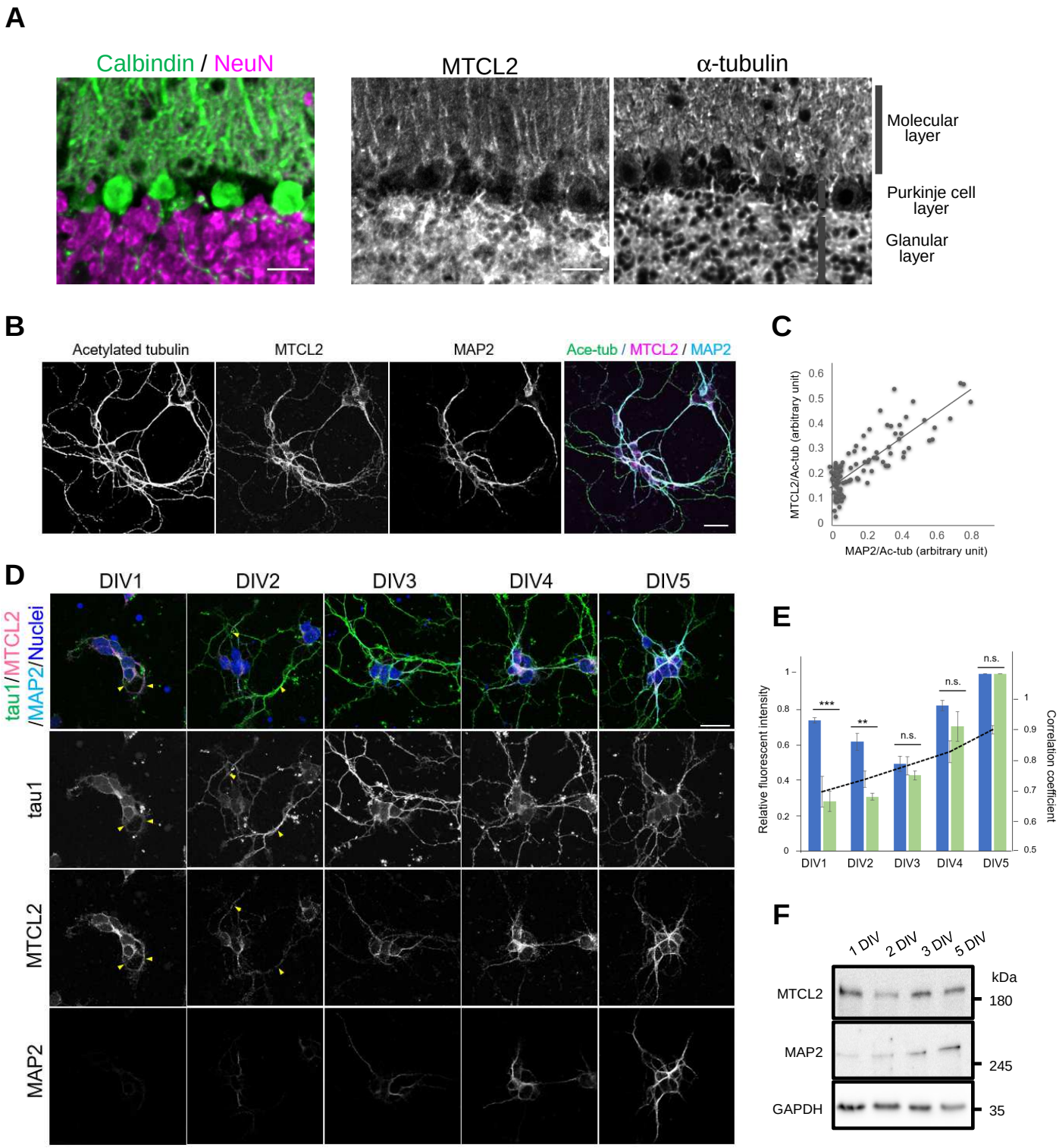
A
Calbindin / NeuN
MTCL2
α-tubulin
Molecular layer
Purkinje cell layer
Glanular layer
B
Acetylated tubulin
MTCL2
MAP2
Ace-tub / MTCL2 / MAP2
C
MTCL2/Ac-tub (arbitrary unit)
MAP2/Ac-tub (arbitrary unit)
D
DIV1
DIV2
DIV3
DIV4
DIV5
tau1/MTCL2/MAP2/Nuclei
tau1
MTCL2
MAP2
E
Relative fluorescent intensity
Correlation coefficient
***
**
n.s.
n.s.
n.s.
DIV1
DIV2
DIV3
DIV4
DIV5
F
1 DIV
2 DIV
3 DIV
5 DIV
kDa
MTCL2
180
MAP2
245
GAPDH
35

Figure 2

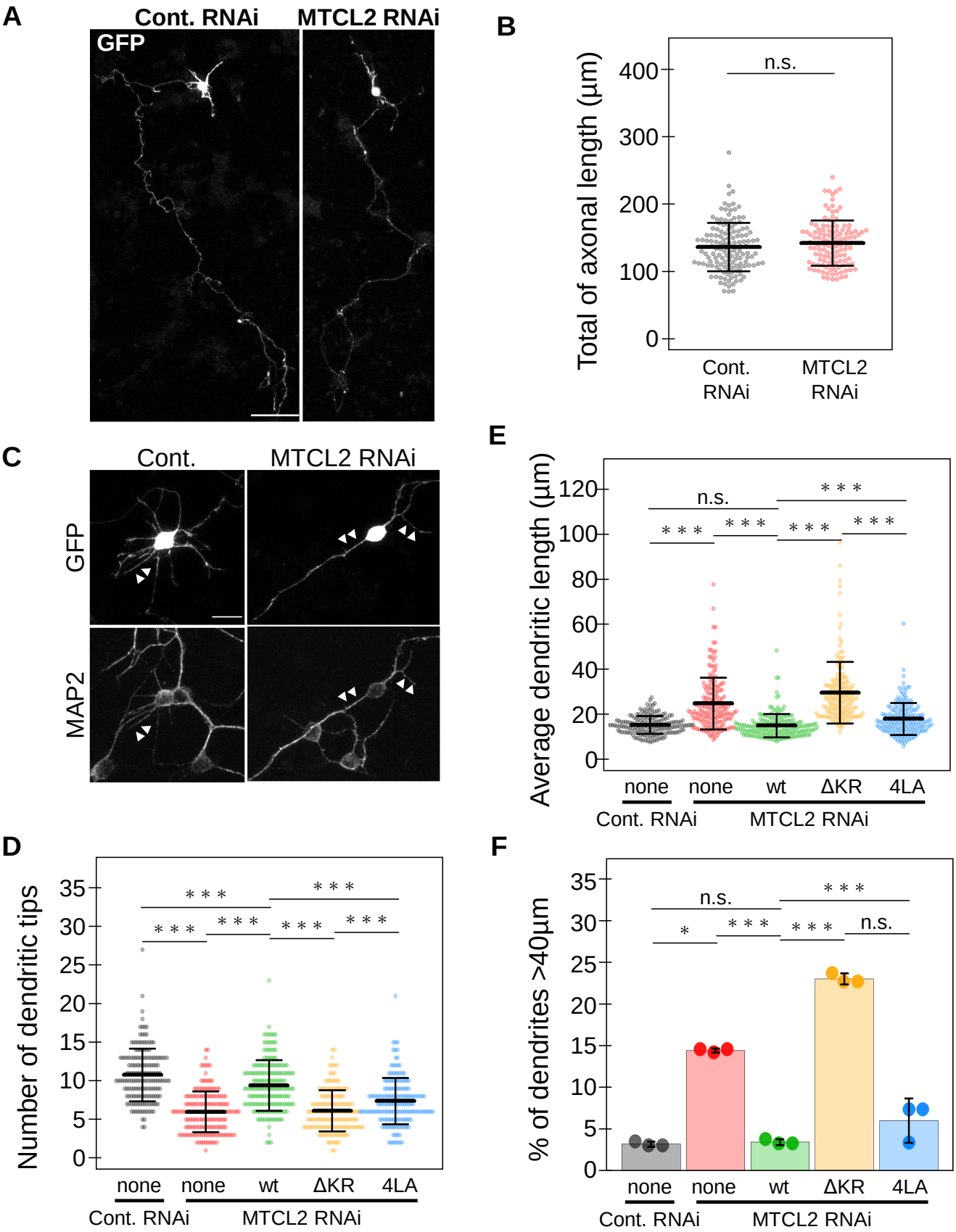
A
Cont. RNAi
MTCL2 RNAi
GFP
B
Total of axonal length (µm)
400
300
200
100
0
n.s.
Cont. RNAi
MTCL2 RNAi
C
Cont.
MTCL2 RNAi
GFP
MAP2
E
Average dendritic length (µm)
120
100
80
60
40
20
0
n.s.
* * *
none
none
wt
ΔKR
4LA
Cont. RNAi
MTCL2 RNAi
D
Number of dendritic tips
35
30
25
20
15
10
5
0
none
none
wt
ΔKR
4LA
Cont. RNAi
MTCL2 RNAi
F
% of dendrites >40µm
35
30
25
20
15
10
5
0
n.s.
*
* * *
none
none
wt
ΔKR
4LA
Cont. RNAi
MTCL2 RNAi

Figure 3

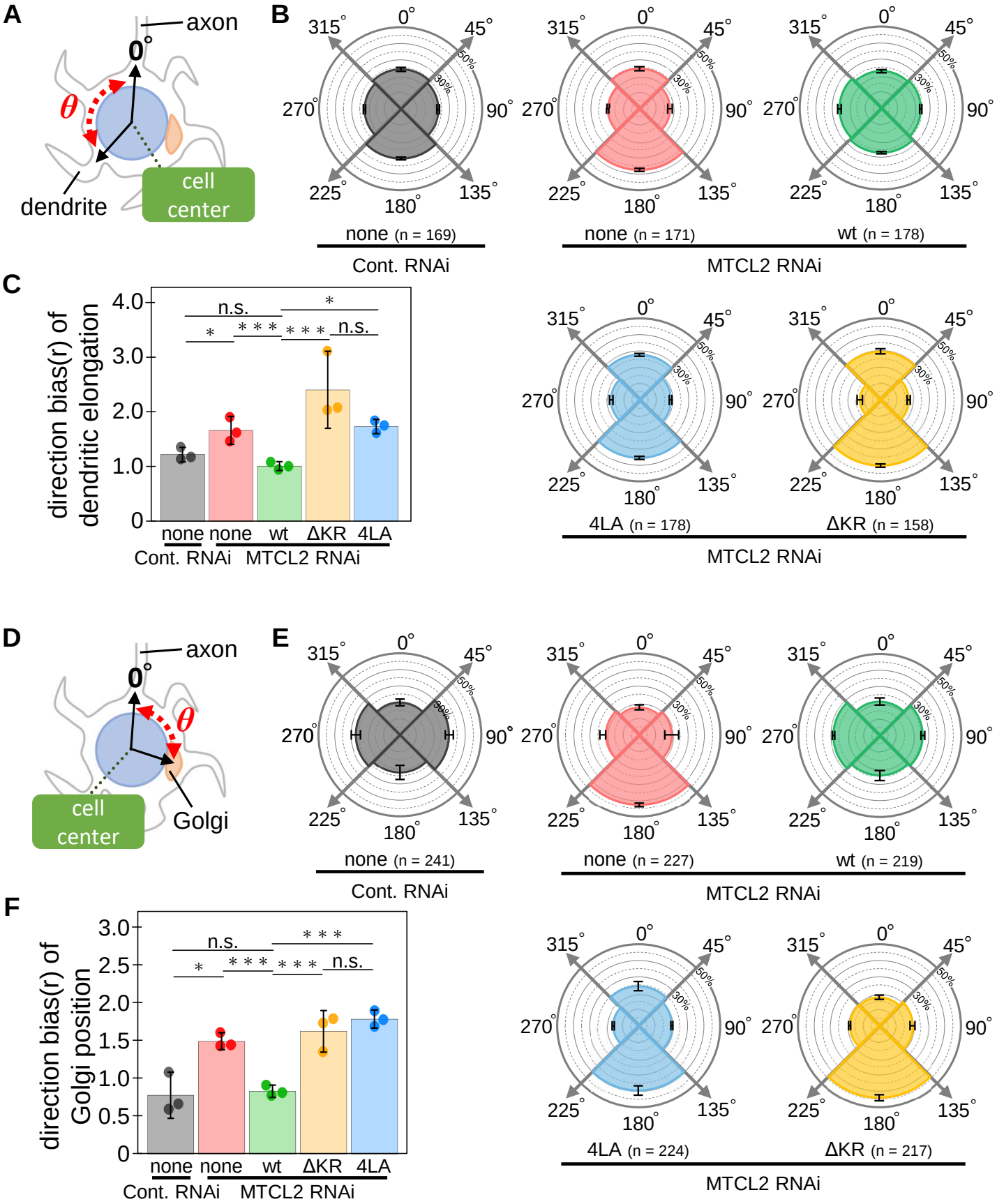
A
axon
0°
θ
dendrite
cell center
B
none (n = 169)
none (n = 171)
wt (n = 178)
Cont. RNAi
MTCL2 RNAi
C
direction bias(r) of dendritic elongation
4.0
3.0
2.0
1.0
0
n.s.
*
* * *
* * *
n.s.
none none wt ΔKR 4LA
Cont. RNAi MTCL2 RNAi
4LA (n = 178)
ΔKR (n = 158)
MTCL2 RNAi
D
axon
0°
θ
cell center
Golgi
E
none (n = 241)
none (n = 227)
wt (n = 219)
Cont. RNAi
MTCL2 RNAi
F
direction bias(r) of Golgi position
3.0
2.5
2.0
1.5
1.0
0.5
0
n.s.
* * *
* * *
* * *
n.s.
none none wt ΔKR 4LA
Cont. RNAi MTCL2 RNAi
4LA (n = 224)
ΔKR (n = 217)
MTCL2 RNAi

Figure 4

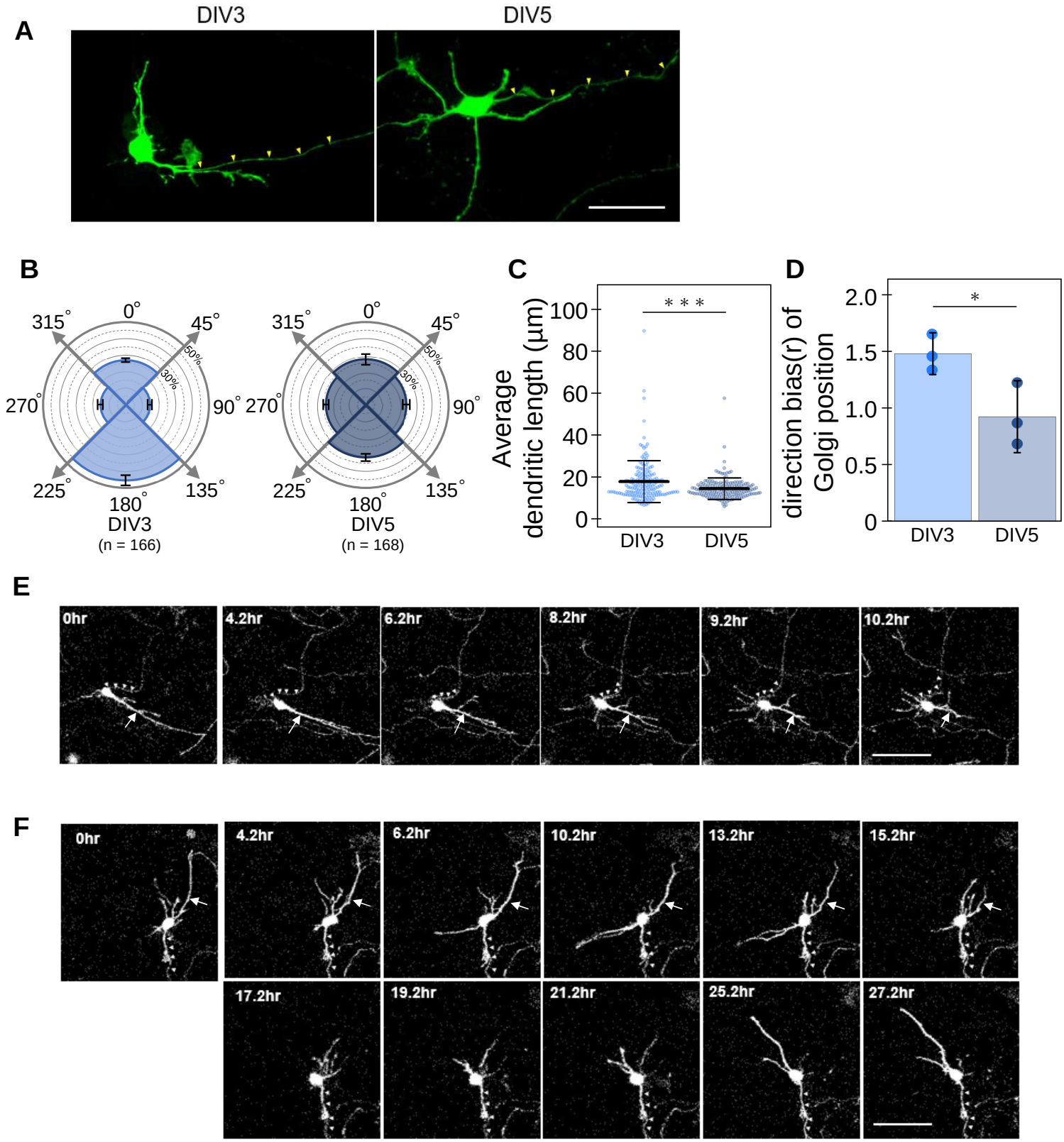
A
DIV3
DIV5
B
0°
45°
90°
135°
180°
225°
270°
315°
30%
50%
DIV3
(n = 166)
DIV5
(n = 168)
C
Average dendritic length (μm)
100
80
60
40
20
0
* * *
DIV3
DIV5
D
direction bias(r) of Golgi position
2.0
1.5
1.0
0.5
0
*
DIV3
DIV5
E
0hr
4.2hr
6.2hr
8.2hr
9.2hr
10.2hr
F
0hr
4.2hr
6.2hr
10.2hr
13.2hr
15.2hr
17.2hr
19.2hr
21.2hr
25.2hr
27.2hr

Figure 5

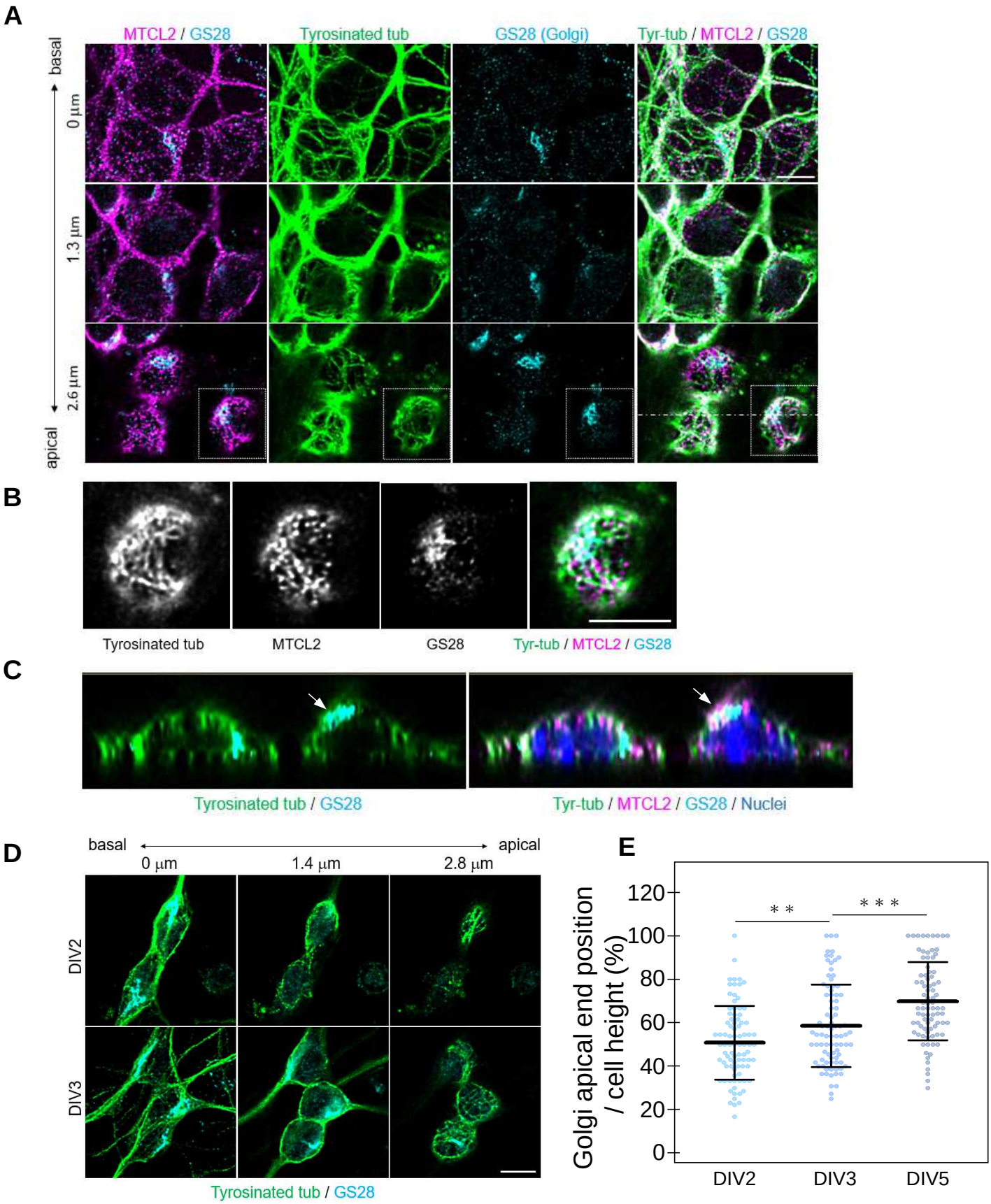
A
MTCL2 / GS28
Tyrosinated tub
GS28 (Golgi)
Tyr-tub / MTCL2 / GS28
basal
0 µm
1.3 µm
2.6 µm
apical
B
Tyrosinated tub
MTCL2
GS28
Tyr-tub / MTCL2 / GS28
C
Tyrosinated tub / GS28
Tyr-tub / MTCL2 / GS28 / Nuclei
D
basal
apical
0 µm
1.4 µm
2.8 µm
DIV2
DIV3
Tyrosinated tub / GS28
E
Golgi apical end position / cell height (%)
120
100
80
60
40
20
0
* *
* * *
DIV2
DIV3
DIV5

Figure 6

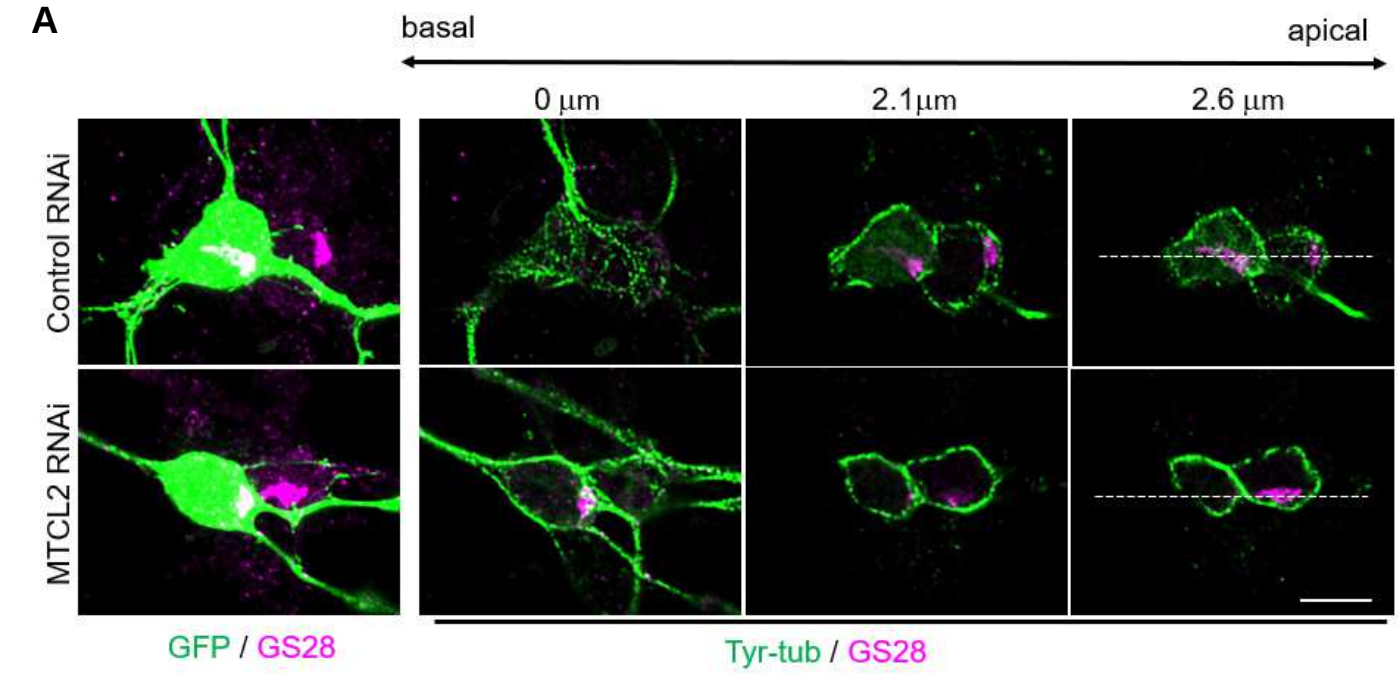
A
basal
apical
0 µm
2.1µm
2.6 µm
Control RNAi
MTCL2 RNAi
GFP / GS28
Tyr-tub / GS28

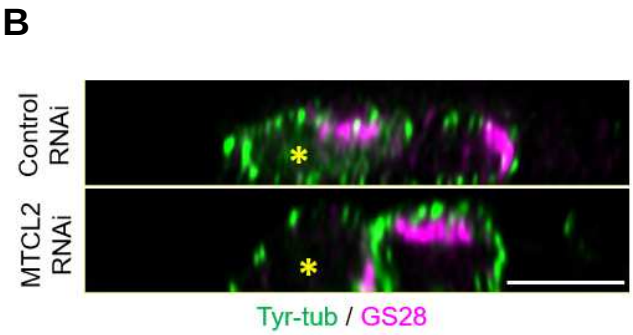
B
Control RNAi
MTCL2 RNAi
Tyr-tub / GS28

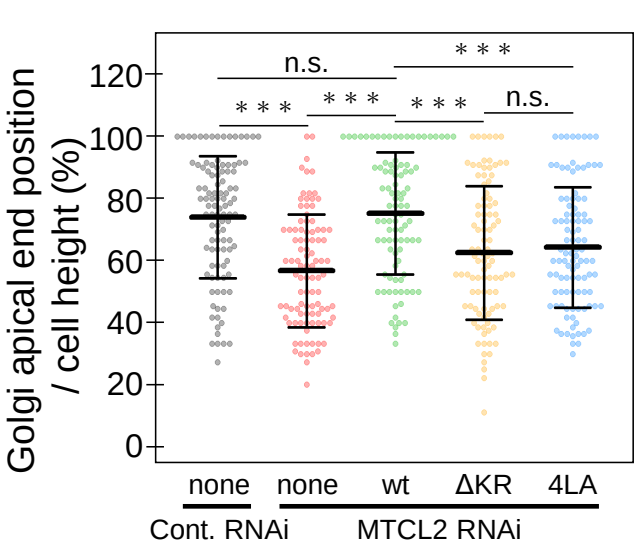
C
Golgi apical end position / cell height (%)
120
100
80
60
40
20
0
n.s.
* * *
* * *
* * *
* * *
n.s.
none
none
wt
ΔKR
4LA
Cont. RNAi
MTCL2 RNAi

Figure 7

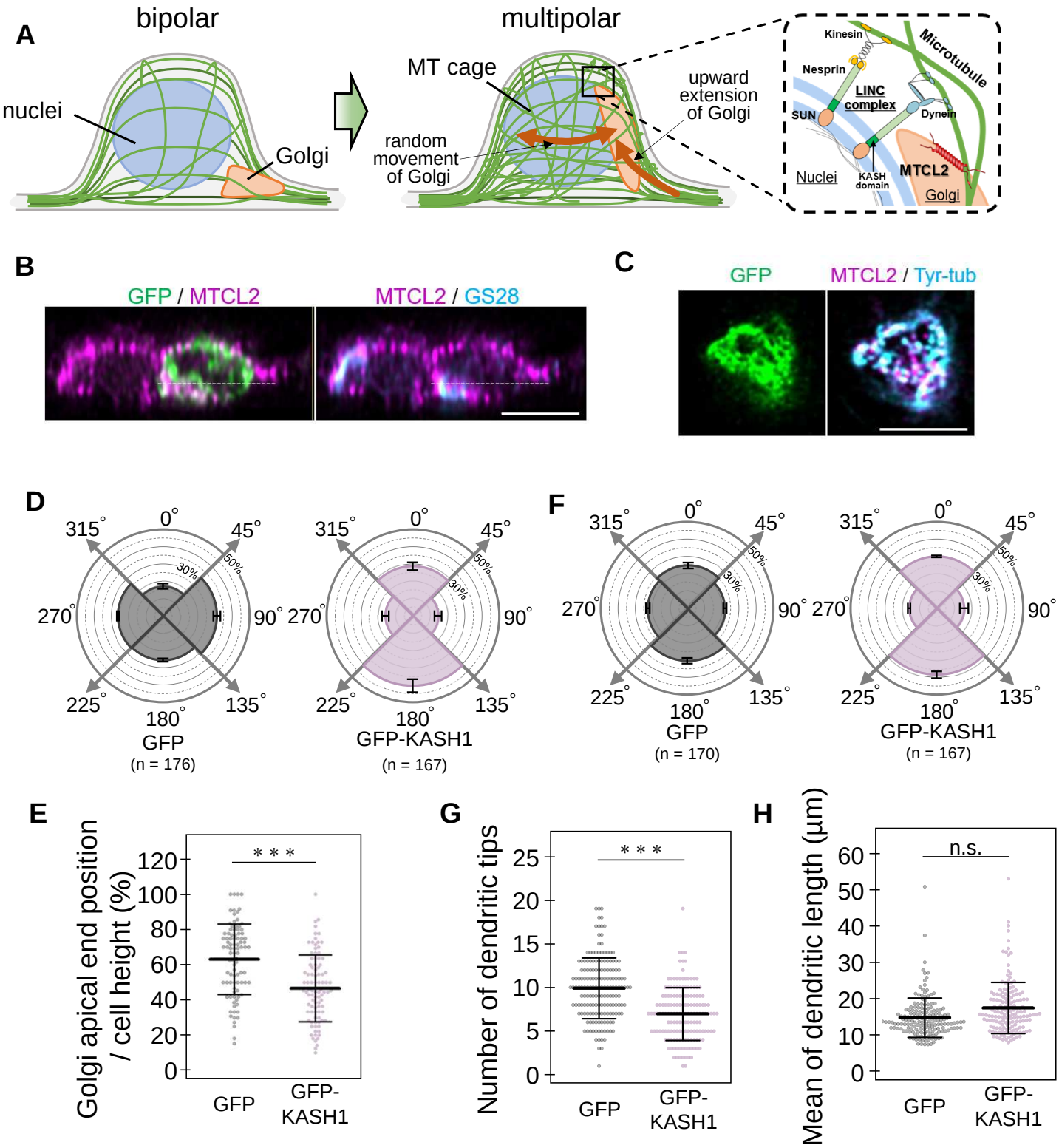
A
bipolar
multipolar
nuclei
Golgi
MT cage
random movement of Golgi
upward extension of Golgi
Kinesin
Microtubule
Nesprin
LINC complex
SUN
Dynein
Nuclei
KASH domain
MTCL2
Golgi
B
GFP / MTCL2
MTCL2 / GS28
C
GFP
MTCL2 / Tyr-tub
D
GFP
(n = 176)
GFP-KASH1
(n = 167)
F
GFP
(n = 170)
GFP-KASH1
(n = 167)
E
Golgi apical end position / cell height (%)
* * *
GFP
GFP-KASH1
G
Number of dendritic tips
* * *
GFP
GFP-KASH1
H
Mean of dendritic length (μm)
n.s.
GFP
GFP-KASH1